Minerals Engineering 201 (2023) 108205

Contents lists available at ScienceDirect

Minerals Engineering

journal homepage: www.elsevier.com/locate/mineng

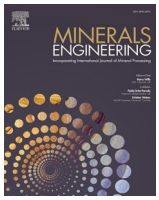

# Vanadium in phyllosilicate ores: Occurrence, crystal chemistry, and leaching behavior

Maxwell Drexler [a,b], Isabel Barton [a,*], Pierre-Marie Zanetta [c]

[a] University of Arizona Department of Mining & Geological Engineering, Tucson, AZ, United States
[b] Now with Rio Tinto Inc., Salt Lake City, UT, United States
[c] Lunar and Planetary Laboratory, The University of Arizona Tucson, AZ, United States

ARTICLE INFO

*Keywords:*
Vanadium leaching
Nanomineralogy
V oxidation state
Geometallurgy
Vanadium in phyllosilicates
Silicate dissolution

ABSTRACT

This article examines the nanoscale occurrence patterns of vanadium in phyllosilicates and correlates them with amenability to leaching. A large fraction of the global vanadium resource is hosted in phyllosilicate ores such as roscoelite and V-bearing chlorites, clays, and micas. Recovery of V from these minerals in acid leaching is typically low but varies widely for unclear reasons. Transmission electron microscopy (TEM) of V-illites, V-chlorites, and roscoelites in leach heads and tails from the La Sal mine (Colorado Plateau) shows that the observed variability in recoveries correlates with intercalations of nanoscale V oxide phases within the phyllosilicate lattice. These are present in some of the V-illites in this study, which displayed higher leach recovery than V-illites without the V oxides. In the latter, as well as in V-chlorites, the V occurs as crystallographic substitutions without oxide intercalations. Electron energy loss spectroscopy (EELS) measurements in the scanning transmission electron microscope (STEM) show that this crystallographic V is mixed-valence, averaging 3.3 in V-chlorite, 3.6 in roscoelite, and 3.8 in V-illite. Unlike the oxide intercalations, this crystallographic type of V corresponds to negligible leaching recoveries irrespective of V siting, oxidation state, or type of phyllosilicate.

These results shed light on the causes of a central problem in geometallurgy, which is attempting quantitative predictions of process outcomes from geological inputs. These results show that what appears to be the same mineral (in this case V-illite) can yield wildly disparate leach recoveries depending on nanoscale metal occurrence factors. Similar under-recognized variation in other ore minerals, within or between sites, may explain much of the notorious variability in their leaching behavior.

## 1. Introduction

### 1.1. Modes of occurrence of metals in phyllosilicates

Metals have three distinct modes of occurrence in phyllosilicates. Metals may occur as non-phyllosilicate mineral phases (e.g. native metals, metal oxides), within the phyllosilicate structure, forming inclusions at the nanoscale (Ilton and Verblen, 1993; Ahn et al., 1997). Metals may also occur as ions adsorbed onto the surfaces of clay minerals. This occurs in nature to some extent but is a particular problem in industry leach settings, where clays and other sheet silicates adsorb metals from pregnant leach solutions, causing preg-robbing (Baum, 1999; Graefe et al., 2017). The third mode of occurrence is metals bonded crystallographically as part of a mineral lattice. Typically tetravalent metal cations such as Ti occupy tetrahedral sites, divalent cations like Ni, Zn, or Fe are found in the octahedral sites, and trivalent cations like Al can be found in either site depending on the mineral and its degree of ordering (Fig. 1). All three modes are relatively common in phyllosilicates (Bleam, 1993; Ahn et al., 1997).

While this is understood at a mineralogical level, connections with extraction behavior are lacking. This represents a major gap in geometallurgical research for some metals. Phyllosilicates can be important ore types, as in the case of V-bearing phyllosilicates in the United States and China (Gao et al., 2021) and for Ni and Zn laterite ores globally (e.g. Borg et al., 2003). Along with exchange of adsorbed metals, the leaching of metal cations from phyllosilicates is a source of especially high acid consumption in heap leaching (Baum, 1999; Jansen and Taylor, 2003, Chetty, 2018). However, not much is known about the nanoscale mechanisms of either metal extraction or acid consumption in phyllosilicates, nor how they relate to the type of occurrence of the metal. This

* Corresponding author.
*E-mail address:* fay1@arizona.edu (I. Barton).

https://doi.org/10.1016/j.mineng.2023.108205
Received 18 November 2022; Received in revised form 15 June 2023; Accepted 18 June 2023
Available online 3 July 2023

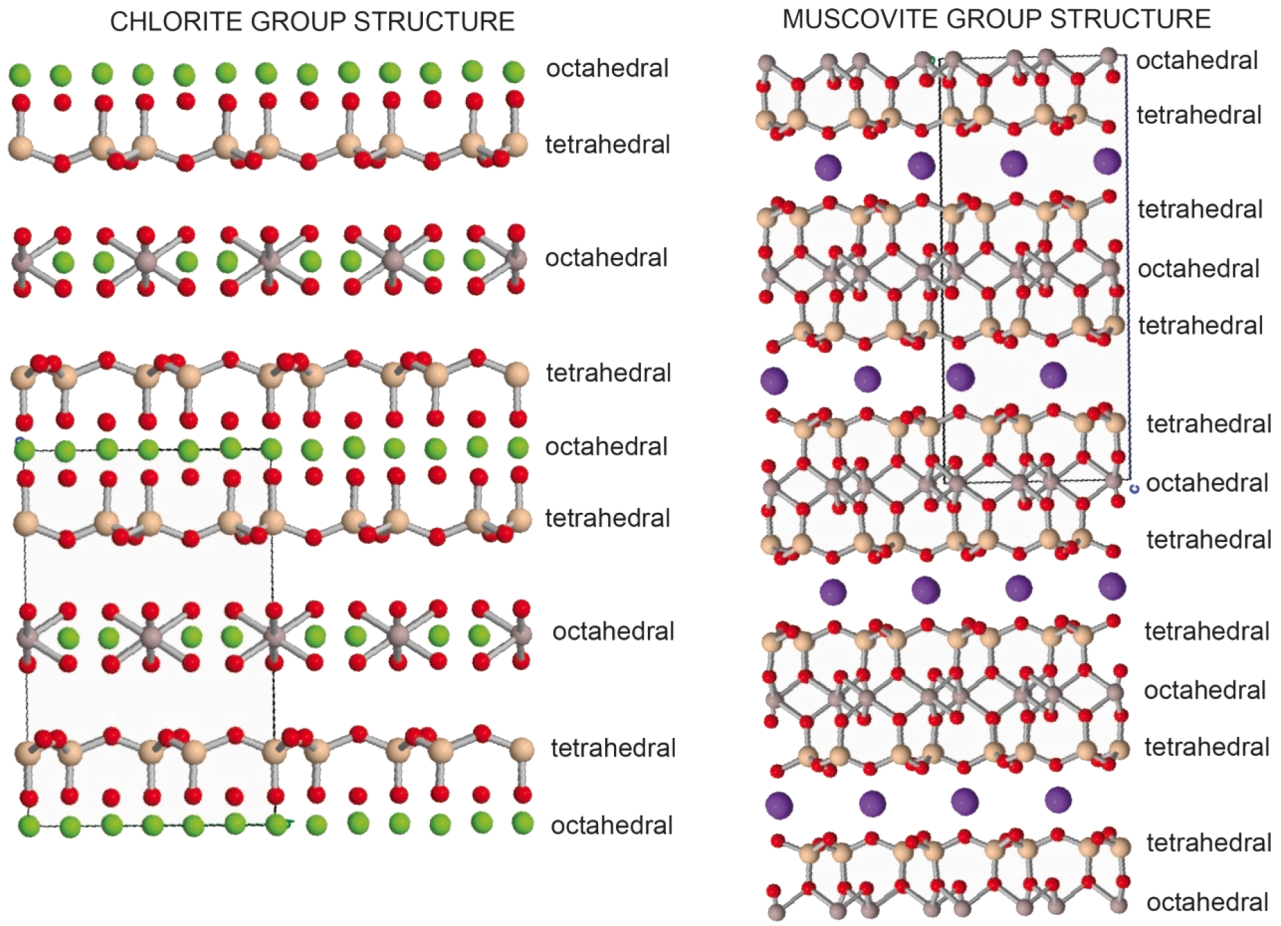


**Fig. 1.** Structures of chlorite and muscovite minerals showing octahedrally and tetrahedrally coordinated sites, from www.mindat.org. View is perpendicular to c-axis and black boxes show unit cell outlines.

study focuses on the occurrence and extraction of V in phyllosilicate minerals as a case study with broader implications for other metals carried by phyllosilicates as well.

### *1.2. Vanadium uses, resources, and production in the United States*

Vanadium's principal use is as a hardening agent in steel, where it improves toughness and wear resistance (Polyak, 2018). Catalysts are the greatest non-alloy use of V, which is listed as a critical mineral by the U.S. Department of the Interior (Polyak, 2018, 2021) and the European Union (European Commission, 2020). In addition, ongoing development of V redox-flow batteries for large-scale energy storage represents a large potential increase in demand if technologies proceed to commercialization (Kear et al., 2011).

Primary V production in the United States mainly comes from Triassic or Jurassic sandstone-hosted uranium deposits in the Paradox Basin on the Colorado Plateau (Gao et al., 2021). In the Paradox Basin the principal V ore minerals are generally a V-hydroxide phase, such as montroseite [(V,Fe)O(OH)] or duttonite ($(V,Fe)O(OH)_2$), and V phyllosilicates such as roscoelite ($K(V,Al)_2(AlSi_3)O_{10}(OH)_2$), V-chlorite ($(V,Fe,Mg,Al)_6(Si,Al)_4O_{10}(OH)_8$), or V-illite ($K_{0.65}(V,Al)_2(Al,Si)_4O_{10}(OH)_2$) (Meunier, 1994; Radwany and Barton, 2022). The geology and mineralogy of these deposits are reviewed by Kerr (1958), Sanford (1992), and more recently by Barton et al. (2018).

### *1.3. Extractive metallurgy of primary vanadium*

Vanadium exists in multiple oxidation states in natural systems. Combinations of V(iii), V(iv), and V(v) may be present in over 300 minerals, forming at least nine ionic complexes in water at 25 °C depending on the redox and pH conditions (Pourbaix, 1975; Gao et al., 2021). This chemical versatility has led to a wide range of possible extraction methods for vanadium ores. The traditional process relied on salt roasting under oxidizing conditions in a rotary kiln or multiple-hearth roaster with NaCl or $NaHCO_3$. Roasting essentially converts the V into water-soluble polyvanadates, which can be leached by hot water leaching or alkali leaching from the calcine (Gupta, 1985). Direct sulfuric acid leaching is also applied to vanadium ores without prior processing, followed by recovery from the leach solution by ion exchange or solvent extraction (Baker and Sparling, 1981; Gupta, 1985). Whereas salt roasting recovers most V from nearly all ore types, direct leaching tends to work well on V (hydr)oxides but poorly on V phyllosilicates (Radwany and Barton, 2022). Though salt roasting was more common in the past when maximizing V recovery was the priority, current US processes use direct leaching since both U and much of the V can be extracted from typical tabular U-V ores at lower cost. More complete overviews of V extraction are available from Gupta and Krishnamurthy (1995), Moskalyk and Alfantazi (2003), and Gilligan and Nikoloski (2020).

The complex mineralogy of V ores poses several challenges for direct leaching, leading to low V recoveries. For example, V recovery by direct sulfuric acid leaching is around 65–71% at the Shaanxi Wuzhou Mining Co., Ltd. in China and around 75% at the White Mesa mill in Utah, USA (Peters Geosciences, 2014; Gao et al., 2021). Uranium recovery at White Mesa is typically 95% and performed at the same grind size and leaching conditions as V (Peters Geosciences, 2014). A recent geometallurgical study attributed this to V deportment. On average, 45% of the V in the deposits in question occurs in readily soluble hydroxide minerals, while

**Table 1**
Calculation of nominal V bond strengths based on the possible coordination and valence of V in phyllosilicates, following Pauling's rules.

| V Redox State | V Coordination Number | Nominal Electrostatic Bond Strength |
|---|---|---|
| $V^{3+}$ | 6 | 0.50 |
| $V^{3+}$ | 4 | 0.75 |
| $V^{4+}$ | 6 | 0.33 |
| $V^{4+}$ | 4 | 1.0 |

55% occurs in phyllosilicates whose recoveries varied strongly in leaching with $H_2SO_4$ and $NaClO_3$ at 25 ℃ (Radwany, 2021). The variation did not appear to correlate with type of V-phyllosilicate or other discernible factors. Even within single types of phyllosilicate, such as V-illite, observed leach recoveries at room temperature varied from 0 to 36% V extraction without apparent reason (Radwany, 2021; Radwany and Barton, 2022).

There is no published information on the extractability or leaching rates of metals that occur in phyllosilicates as native species or oxide inclusions. Most leaching and dissolution studies on phyllosilicates do not apply STEM-EELS or other techniques capable of detecting such nanoscale inclusions and quantifying their crystal chemistry, leaving their possible role in metal dissolution unknown.

### 1.4. This study

This work investigates the leaching of V-bearing phyllosilicate minerals, partly to identify the causes of the observed variability in leach results (Radwany, 2021) and partly as a broader case study of the behavior of phyllosilicates in acid leaching (Drexler, 2022). Major questions include (1) the occurrence of V and its oxidation state in phyllosilicates at the nanoscale, (2) the evolution of V in phyllosilicates over the course of acid leaching, and (3) how V occurrence patterns affect leaching results. For instance, one of the objectives of this study is to investigate the correlation between the crystal chemistry of a metal and its extractability. In theory, tetrahedral V(iv) should be much more refractory to leaching than octahedral V(iii) due to higher bond strength (Table 1), and so with other metals. While this has been examined on a theoretical basis in the past (Osthaus, 1953; Ross, 1969; Terry, 1983a,b), detailed recent studies with experimental data are lacking.

## 2. Materials and methods

### 2.1. Sample provenance and characterization

Samples of uranium and vanadium phyllosilicates for this project came from the ore head samples and leach residues of experimental work conducted by Radwany (2021). Six ore samples (LS01, LS02, LS03, LS04, LS05, and LS11) were collected from the Pandora mine in the La Sal mining complex, representing the common Salt Wash-hosted tabular type of U-V ore deposit (reviewed by Dahlkamp, 2010; Cuney et al., 2022). The rocks were crushed, ground, and split, with some splits of each sample mounted in epoxy for mineralogical analysis and others designated for leach testing. The full accounts of sample types, prep operations, and geological context are given in Radwany (2021) and Radwany and Barton (2022).

Thin sections of three of the six samples were made for optical petrographic characterization. For each of the six samples, a total of 56 elements were analyzed using ICP-OES/MS after four-acid digestion, with a LECO carbon combustion assay as well. Semi-quantitative mineralogical information of the samples came from analysis by the Tescan TIMA3 field emission SEM analyzer at the Freeport-McMoRan Tucson Technology Center. For details of the analytical methods and an analysis of the results, see Radwany (2021).

The samples are relatively pure, mainly quartzose sandstones with minor feldspar, lithic clasts, and irregular but small amounts of coalified plant material, calcite, and heavy minerals such as anatase (Bos-Orent, 2021; Radwany, 2021). Vanadium and uranium oxides are found as tiny grains (<5 μm) partly or fully enclosed within quartz rims, and more commonly as larger (mm-scale) interstitial fillings between grains. Much of the rock matrix is V-phyllosilicates, which act as a cement (Radwany, 2021).

**Table 2**
Select whole-rock elemental assays of the six ore samples. b.d. = below detection limit. ACT = acid consumption (Radwany, 2021).

| Sample | LS01 | LS04 |
|---|---|---|
| Al (%) | 0.65 | 1.97 |
| C (%) | *b.d.* | *b.d.* |
| Ca (%) | 0.06 | 0.09 |
| Fe (%) | 0.40 | 0.86 |
| K (%) | 0.31 | 0.34 |
| Mg (%) | 0.10 | 0.86 |
| Na (%) | *b.d.* | 0.08 |
| P (%) | 0.01 | 0.01 |
| S (%) | 0.13 | 0.13 |
| Ti (%) | 0.02 | 0.15 |
| U (%) | 0.05 | 0.19 |
| V (%) | 1.95 | 1.87 |
| Total ACT (lb/t) | 114 | 87 |
| V/U | 37.6 | 10.1 |

**Table 3**
Semiquantitative modal mineralogy as determined by Tescan TIMA. Average and one standard deviation are among three replicates for each sample. Dash indicates the phase occurs as <1% by volume. Phases detected at <1% in all samples are not listed (Radwany, 2021).

| Phase | LS01 | *LS01 σ* | LS04 | *LS04 σ* |
|---|---|---|---|---|
| Quartz (%) | 89.1 | *0.56* | 81.6 | *0.46* |
| V-phyllosilicates (%) | 8.9 | *0.50* | 14.8 | *0.37* |
| V-hydroxide (%) | 1.8 | *0.04* | 1.2 | *0.08* |
| U minerals (%) | – | – | – | – |
| K-feldspar (%) | – | – | 1.1 | *0.09* |
| All other minerals (%) | 0.19 | *0.01* | 1.23 | *0.04* |

The focus of this study was on two samples LS01 and LS04, selected because they represent two types of V-phyllosilicate (illite and chlorite respectivelly) and two levels of recovery as determined by Radwany (2021). The chemical and mineralogical compositions of the overall samples are shown in Tables 2-3.

### 2.2. Summary of previous leach testing and results

To investigate the geometallurgical behavior of the sampled ores, they were leached in stirred beakers at pH < 2 using 10 g/L $H_2SO_4$ as a lixiviant and 1 g/L $NaClO_3$ as an oxidant, mimicking a current industrial process (Radwany, 2021). The oxidant kept the Eh between 600 and 800 mV vs. Ag/AgCl. The experiments were done with 5 wt% solids at room temperature and agitated with a magnetic stir bar. Samples of the lixiviant solution were taken during the leach tests after 10, 20, 30, 60, 120, and 180 min of active leaching time using a syringe equipped with a 1 μm filter (Radwany, 2021). Leach recovery typically reached a plateau around 100–120 min, indicating that this time was sufficient to achieve ultimate room-temperature recovery. Residues from the experiments (leached tails) were filtered, rinsed in deionized water, dried, and epoxy mounted for electron microprobe observation. After a 1:150,000 dilution, the solutions were analyzed at the University of Arizona Economic Geology and Geometallurgy lab using a ThermoFisher Element2 ICP-MS respectively and compared to the unleached head.

For sample LS01, 53% of V leached in the acidic beaker test, compared to 14% for sample LS04 (Radwany, 2021). Electron microprobe analysis of the unleached heads and leached tails showed that

**Table 4**
Comparative head and residue analyses (Wt%) of V-phyllosilicates leached in this study. Modified from Radwany (2021).

| **V-chlorite** | | | | | | | | | | | | | | |
|---|---|---|---|---|---|---|---|---|---|---|---|---|---|---|
| **Sample #** | **Material** | **Phase** | **Na** | **Mg** | **Al** | **Si** | **K** | **Ti** | **Ca** | **V** | **Fe** | **U** | **O** (calc) | **Total** |
| **LS04** | Head | V-chlorite | 0 | 5.9 | 12 | 16.5 | 0.7 | 0 | 0 | 8.9 | 5 | 0 | 39.2 | 88.5 |
| **LS04** | Head | V-chlorite | 0 | 4.7 | 10.6 | 16.9 | 1.8 | 0.1 | 0.1 | 10.2 | 4.1 | 1.7 | 38.5 | 88.7 |
| **LS04** | Head | V-chlorite | 0.1 | 4 | 10 | 14.2 | 0.9 | 0.1 | 0.1 | 16.6 | 8 | 1.2 | 38.3 | 93.6 |
| **LS04** | Head | V-chlorite | 0.2 | 3.7 | 8 | 11.7 | 1.1 | 0.6 | 0 | 20.5 | 6.6 | 2.8 | 35.5 | 90.6 |
| **LS04** | Tail | V-chlorite | 0 | 6 | 11.9 | 15.9 | 0.8 | 0.2 | 0 | 7.8 | 4.6 | 0 | 38 | 85.5 |
| **V-illite** | | | | | | | | | | | | | | |
| **Sample #** | **Material** | **Phase** | **Na** | **Mg** | **Al** | **Si** | **K** | **Ti** | **Ca** | **V** | **Fe** | **U** | **O** (calc) | **Total** |
| **LS01** | Head | V-illite | 0.2 | 0.7 | 9.8 | 17.7 | 6.2 | 0.1 | 0 | 17.7 | 1.3 | 0 | 39.4 | 93 |
| **LS01** | Head | V-illite | 0.1 | 1.5 | 11.2 | 20 | 5.7 | 0.1 | 0 | 11.6 | 1.4 | 0 | 40.9 | 92.6 |
| **LS01** | Head | V-illite | 0.1 | 0.6 | 9.1 | 18.5 | 6 | 0 | 0 | 16.9 | 1.5 | 0.1 | 39.2 | 92.3 |
| **LS01** | Head | V-illite | 0.5 | 0.6 | 8.5 | 17.1 | 5 | 0.1 | 0 | 20.2 | 1.8 | 0 | 38.7 | 92.5 |
| **LS01** | Tail | V-illite | 0 | 0.5 | 7.7 | 19 | 5.7 | 0 | 0 | 10.5 | 1 | 0 | 39.9 | 84.3 |
| **LS01** | Tail | V-illite | 0 | 0.5 | 9.1 | 20.3 | 6.3 | 0 | 0 | 11.4 | 0.8 | 0 | 39.7 | 88.1 |
| **LS01** | Tail | V-illite | 0.1 | 1.5 | 10.1 | 22.8 | 5.1 | 0.1 | 0.1 | 6.4 | 2.4 | 0 | 40.8 | 89.4 |

liberated V-(hydr)oxides dissolved under the experimental conditions, but V-bearing phyllosilicates were present in the tails and showed variably poor V extraction. In the LS01 sample, about 36% of the V was extracted from the phyllosilicates, the highest of the samples tested. Extractions of V from other V-illites in samples LS02, LS03, and LS05 ranged from only 2–18%, for reasons that were not clear in that study (Radwany, 2021). Extraction of V from the V-chlorites in LS04 was negligible. Table 4 gives the EPMA compositions of the V-phyllosilicates in LS01 and LS04 before and after leaching from select grains.

### 2.3. Analytical methods in this study

A benchtop JEOL 6010LA SEM in the University of Arizona Economic Geology and Geometallurgy laboratory was used to select phyllosilicate grains appropriate for S/TEM analysis. Operating conditions were 20 kV accelerating voltage and 10 mm working distance. Grains were imaged using a backscattered electron dectector and selected based on EDS analysis of Al, Si, K, Mg, Fe, and V contents in ratios corresponding to V-phyllosilicates, combined with morphological features such as obvious sheet structures.

This study applied two methods of preparing grains for S/TEM work. Grains for general analyses were prepared by dispersion. Samples of unleached heads and residues from previous leach tests (Radwany, 2021) were crushed in dry conditions in a mortar and pestle and sprinkled onto lacey-carbon films supported by Cu-mesh TEM grids. The grid was then inverted to release large and poorly adhered particles, leaving the smallest particles behind. These typically included enough submicron-sized particles for successful STEM analysis, and most were electron-transparent (<50–100 nm) in at least some areas.

To target specific grains and preserve their mineralogical context in the sample, the authors additionally created TEM lamellae using an FEI Helios dual-beam Nanolab 660 focused ion beam (FIB) SEM located in the Kuiper Materials Imaging and Characterization Facility (KMICF) at the Lunar and Planetary Laboratory, University of Arizona. To protect the sample lamellae from ion beam damage during ion milling, a carbon capping layer of thickness near 500 nm was first deposited with the electron beam at a voltage of 2 kV and current of 3.2nA. Then, a second carbon capping layer of 2–3 μm thickness was deposited using the ion beam under an accelerating voltage of 30 kV and current of 0.32nA. After extraction, each lamella was welded to a copper TEM grid with Pt deposition and thinned with the ion beam under an accelerating voltage of 30 kV and current of 2.5nA to reach a thickness around 100 nm. Final thinning steps to achieve thickness < 100 nm, used progressively decreasing currents and voltages to assure that the lamella remained free of beam damage that could amorphized areas of the sample. Final thinning passes were done with an accelerating voltage of 8 kV and current from 25 to 40 pA.

The thinned lamellae and the samples sprinkled onto lacey-carbon films were measured using a 200 keV aberration-corrected Hitachi HF5000 scanning TEM (S/TEM) located in the Kuiper Materials Imaging and Characterization Facility at the Lunar and Planetary Laboratory, University of Arizona. The HF5000 is equipped with a cold-field emission gun, a third-order spherical aberration corrector, bright-field (BF) and high angular anular dark-field (HAADF) detectors, and two

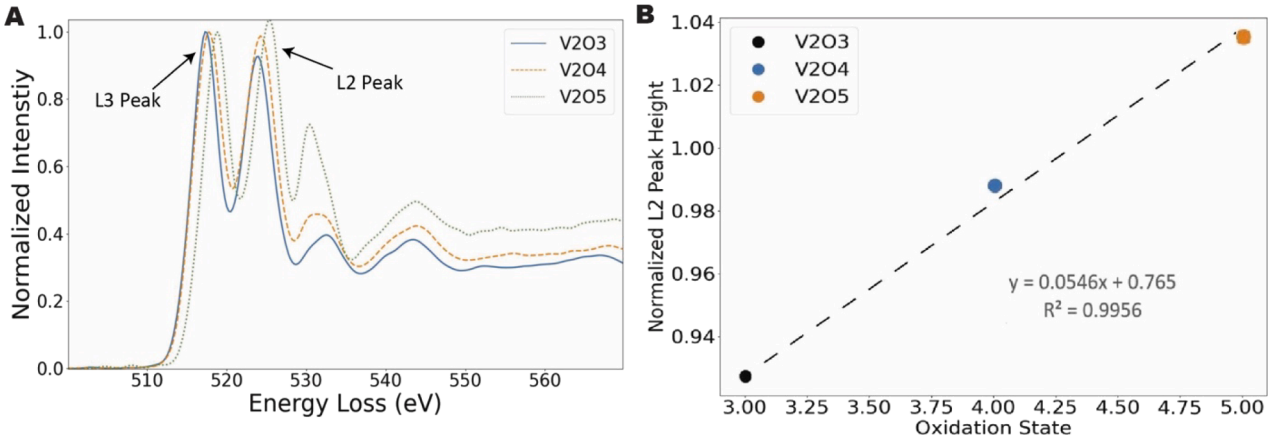


**Fig. 2.** A: EELS spectra for three V standards, processed as described above. Spectra are normalized to the $L_2$ peak height. B: $L_3$ Peak height vs. V oxidation state of $V_2O_3$, $V_2O_4$, and $V_2O_5$ standards after normalization of the individual spectra to their maximum $L_2$ peak height as described by Zanetta et al. (2023).

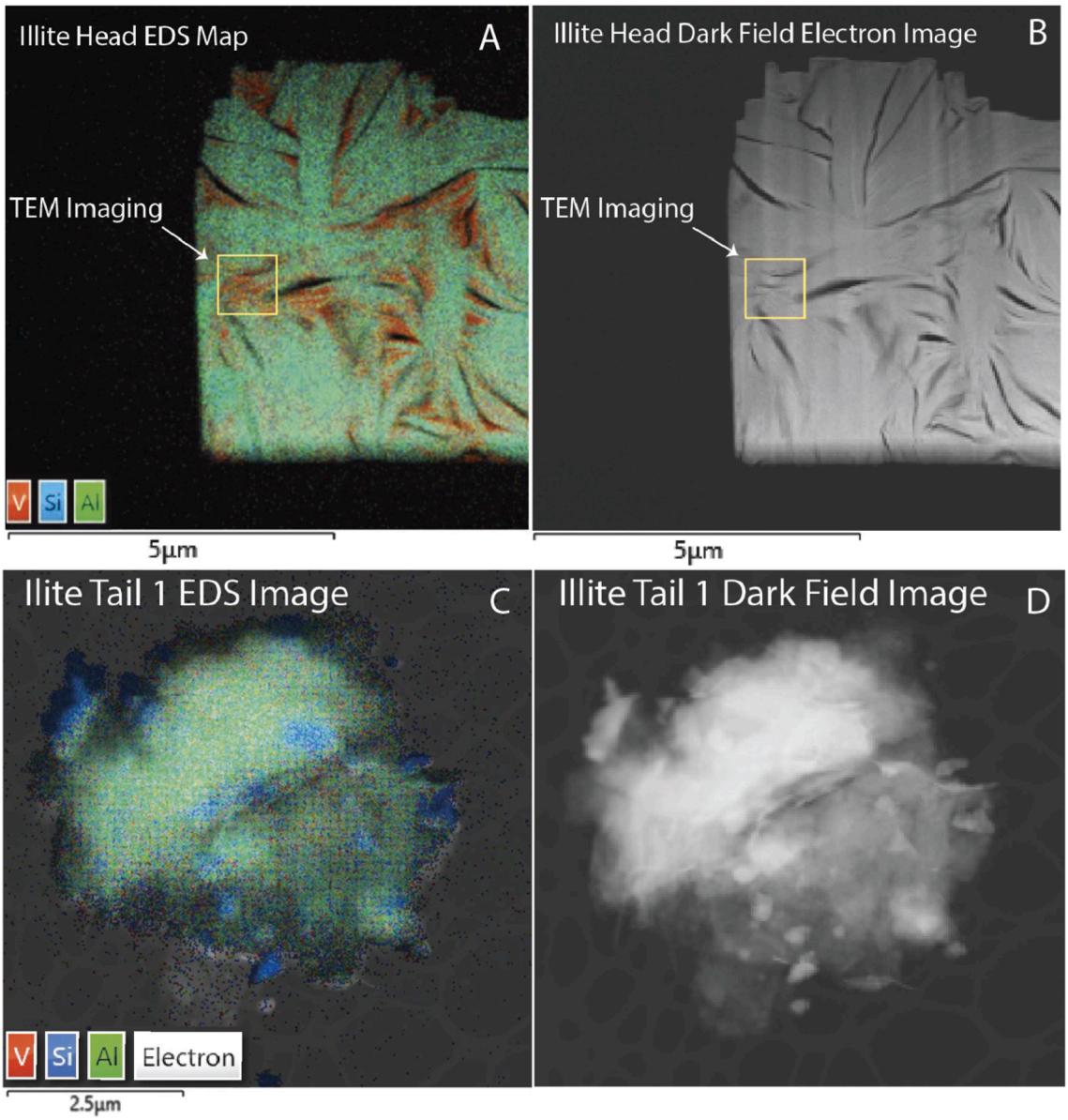


**Fig. 3.** Comparison of the EDS mapping and corresponding dark field electron images of the illite LS01 heads (A-B) and tails (D-E). A,B)high-V areas or edge phases (red on EDS map) are observed and correlated to lower Al and Si concentrations. High-magnification TEM imaging of a high-V area, shown in Fig. 4, was done within the yellow box. C,D) The particle do not show high V areas. Some regions show higher intensity in Si.Most of the material is homogeneous. (For interpretation of the references to colour in this figure legend, the reader is referred to the web version of this article.)

spectrometers: (1) an Oxford Instruments X-Max 100 TLE EDS system including twin, 100-$mm^2$ silicon-drift detectors and (2) a Gatan GIF Quantum ER (model 965) electron energy-loss spectrometer (EELS). The Quantum ER is a Gatan Imaging Filter equipped with a CCD detector and dual EELS capabilities, allowing low-loss and high-loss spectra to be acquired simultaneously.

For EELS, an entrance aperture of 2.5 mm and dispersion of 0.25 eV/channel provided acceptable resolution and a good signal-to-noise ratio. A series of standards (synthetic $V_2O_3$, $V_2O_4$, and $V_2O_5$) was measured to establish a relationship between the V oxidation state and EELS V $L_{2,3}$ features. A nearly stoichiometric natural roscoelite from the Omega mine dumps near Placerville, CO was also measured to compare V EELS spectra in silicates to those in oxides. Spectra were processed using the HyperSpy open-source Python library (de la Pena et al., 2021; Zanetta et al., 2023). Zero loss peak centering was use to calibrate the energy of the low loss and high loss spectra from different pixels and background signal was removed. The intensities of each spectrum were normalized to the $L_3$ peak intensity to remove the contribution of the thickness and of V concentration. The plural scattering contributions due to sample thickness were removed by Fourier-ratio deconvolution.

Processing methods to relate EELS $L_{2,3}$ features into V oxidation states are described by Zanetta et al. (2023) and are summarized here. The $L_2$ peak maximum intensity, normalized to the $L_3$ peak intensity, increase as the oxidation state increase (Fig. 2A). This result is used to establish the calibration curve shown in Fig. 2B. The application of the same procedure on LS01 and LS04 samples allow to determine their oxidation states once projected on the calibration curve.

## 3. Results

### 3.1. V-bearing illites

The V-illite in the LS01 unleached head samples turned out to be composites consisting of multiple, variably oriented phyllosilicate

**Table 5**
EDS results for all samples analyzed on the Hitachi HF-5000 S/TEM expressed as oxide weight percentages.

| Sample | LS01Illite Head | LS01Illite Tail 1 | LS01Illite Tail 2 | LS04 Chlorite Head 1 | LS04Chlorite Head 2 | LS04*Chlorite Head 3 | LS04Chlorite Tail 1 | LS04*Chlorite Tail 2 | LS04Chlorite Tail 3 |
|---|---|---|---|---|---|---|---|---|---|
| Oxide (wt%) | | | | | | | | | |
| $SiO_2$ | 41.2 | 53.8 | 51.4 | 34.0 | 43.4 | 65.3 | 54.8 | 41.7 | 40.5 |
| $Al_2O_3$ | 17.4 | 18.9 | 16.6 | 27.4 | 22.2 | 15.5 | 20.9 | 25.0 | 23.8 |
| $V_2O_3$ | 29.6 | 16.1 | 20.7 | 14.1 | 17.1 | 6.7 | 9.4 | 10.8 | 14.0 |
| $K_2O$ | 7.9 | 8.2 | 7.7 | – | 3.2 | 0.5 | 3.2 | 1.3 | 0.7 |
| MgO | 1.0 | 1.0 | 0.8 | 15.7 | 7.9 | 6.6 | 6.7 | 11.5 | 10.5 |
| $TiO_2$ | – | 0.5 | 0.5 | – | – | 0.9 | 0.4 | – | 2.9 |
| FeO | 2.9 | 1.5 | 2.3 | 7.3 | 6.2 | 4.4 | 4.6 | 9.0 | 7.6 |
| S | – | – | – | – | – | – | – | 0.7 | |
| Sigma (wt%) | | | | | | | | | |
| $SiO_2$ | 0.07 | 0.14 | 0.13 | 0.12 | 0.44 | 0.26 | 0.19 | 0.2 | 0.11 |
| $Al_2O_3$ | 0.06 | 0.11 | 0.10 | 0.11 | 0.39 | 0.20 | 0.15 | 0.18 | 0.1 |
| $V_2O_3$ | 0.07 | 0.11 | 0.11 | 0.04 | 0.36 | 0.15 | 0.12 | 0.15 | 0.09 |
| $K_2O$ | 0.05 | 0.09 | 0.08 | 0.04 | 0.19 | 0.07 | 0.08 | 0.07 | 0.03 |
| MgO | 0.02 | 0.05 | 0.04 | 0.09 | 0.29 | 0.15 | 0.11 | 0.15 | 0.07 |
| $TiO_2$ | – | 0.04 | 0.04 | – | – | 0.07 | 0.05 | – | 0.05 |
| FeO | 0.04 | 0.05 | 0.06 | 0.09 | 0.28 | 0.14 | 0.10 | 0.15 | 0.07 |
| S | – | – | – | – | – | – | – | 0.07 | – |

* Chlorite Head 3 contains a quartz grain, and Chlorite Tail 2 contains a pyrite grain.

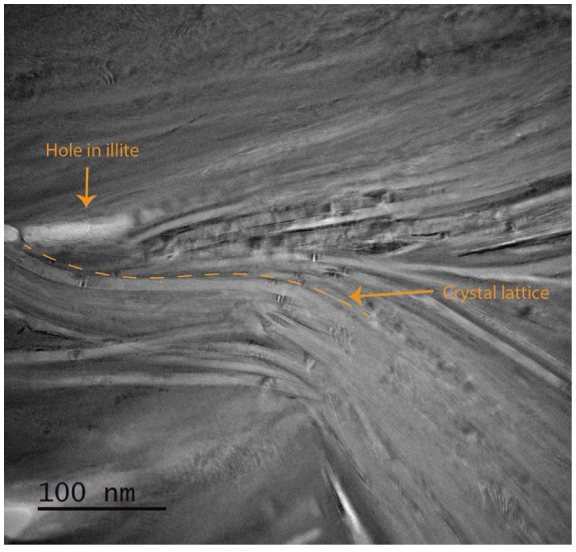


**Fig. 4.** High-V edge phases in the LS01 illite, in 120kX magnification bright-field image in TEM mode (parallel beam). In areas where the sample orientation is favorable, the layered lattice can be seen running approximately E-W across the image. For location of this inset image see Fig. 3A-B.

lattices (Fig. 3A-B). Compositions averaged 29.6 wt% $V_2O_3$ (Table 5), but EDS mapping showed a heterogeneous distribution of Fe, V, Si, and Al. Generally, areas of higher V and Fe concentration occur in proximity to void spaces in the lamella and correlate inversely with areas of higher Si and Al concentration (Fig. 3A).

The extent of compositional heterogeneity suggests that the high-V-Fe, low-Al-Si areas (termed "high-V edge phases") could represent either a separate mineral phase, probably a V(-Fe) oxide, or extreme degrees of coupled substitution in the illite lattice. One possible candidate for a separate phase is nanoscale V(-Fe) oxides, which would be consistent with the results of TEM work on Cu in illites (Ahn, 1997). Similar V(-Fe) oxides are observed at multiple scales in tabular U-V deposits of this type, including La Sal (Barton et al., 2018a,b; Radwany and Barton, 2022). A second possible cause could be extreme degrees of substitution of metals for each other within the phyllosilicate crystal lattice. To investige the nature of the high-V edge phases in the LS01 illite, the authors used higher-resolution TEM imaging in the area shown inside the yellow box in Fig. 3A. The results (Fig. 4) show a strongly layered lattice texture to the high-V edge phases (the beam is oriented perpendicular to the c-axis). The results did not support identifying distinctly separate phases interlayered with the phyllosilicate lattice in the style of native copper inclusions observed by Ahn et al. (1997).

Electron imaging and EDS analysis of illite tail grains dispersed on lacey carbon film from LS01 leaching revealed that V contents were significantly lower than in the head sample at 16.1 to 20.7 wt% $V_2O_3$ (Fig. 3 C,D and Table 5). Distribution of metals is also much less heterogeneous than in the head samples, with variability limited to about ±5 wt% V. Overall, the tail grains retain much of their original content of crystallographically bound metals, including V. The principal difference between heads (Fig. 3A-B) and tails (Fig. 3C-D) is that the tails contain no observed examples of the high-V edge phases. This likely accounts for the difference in V content. Si enrichment is observed, but most of the grain is homogeneous in composition.

The STEM-EDS map of the LS01 head sample at the atomic scale (Fig. 5) shows that most of the V is associated with Fe as a separate oxide, likely a montroseite with approximate formula $(V^{3+}_{0.5}Fe^{3+}_{0.3}V^{4+}_{0.1})O(OH)$. It has a mixed valence and is embedded in the phyllosilicate at the nanoscale. TEM-EELS results support identification of this phase as an oxide distinct from the phyllosilicate (see section 5.3 below). In addition to this separate oxide, some of the V is also in the crystallographic lattice and shows corresponding peaks in the Fig. 5 profile. A Si-rich and V and Al depleted roscoelite (blue areas in the composite image Fig. 5) is also interlayered with the V-rich roscoelite (red areas, Fig. 5).

### 3.2. V-bearing chlorites

Three LS04 tail V-chlorite grains dispersed on the lacey carbon film were analyzed by electron imaging and EDS (Fig. 6). Separate phases observed include quartz, pyrite, and a Ti-V oxide. Anomalously high-V zones of the sample correlate only with Ti, suggesting discrete Ti-V oxides rather than the V-Fe edge phase found in the V-illites. Notably, the high-V edge phases identified in the LS01 V-illites (Fig. 3A-B) were not found in any of the chlorite heads (Fig. 6). STEM-EDS quantification of the three grains from the LS04 head sample show the chlorites contain more Fe and Mg, and less V, than the LS01 illites.

### 3.3. Electron energy loss spectroscopy (EELS) results

To determine the oxidation state and its possible correlation with the geometallurgical behavior of the sample during leaching processes, we

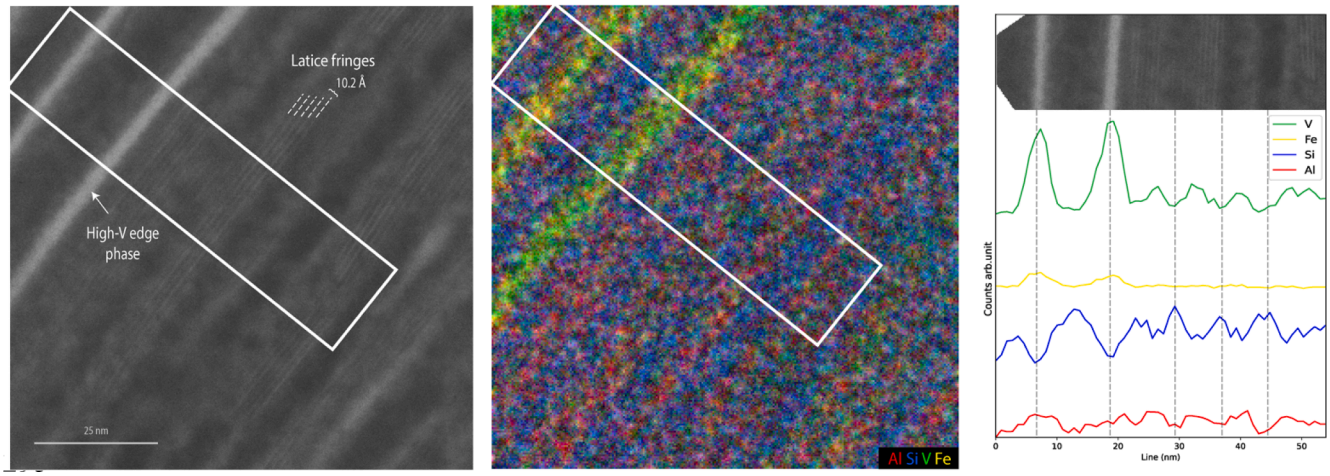


**Fig. 5.** STEM-EDS map of the LS01 illite head sample atomic lattice and the high-V edge phase (Fig. 4). Most of the V is associate with Fe as a separate oxide. The white rectangle represents the profile that is vertically integrated to produce the spectra on the right plot.

measured the oxidation state of V in our samples using EELS (see section 3.3). Results are summarized in Tables 6-7 and Fig. 7. All samples plot as a mixture of V(iii) and V(iv). The V-chlorites (LS04) are the most reduced with an average V oxidation state of + 3.23. The V-illites (LS01) are the most oxidized at + 3.83 on average, and the Placerville roscoelite plots in between at + 3.61 (Table 7). The standard deviation of the data was measured at 0.28, approximately equal to the difference between the average oxidation states in V-illite and V-chlorite.

The EELS data also show that the spectra of the high-V edge phases present in the LS01 Illite 1 Tail sample are distinct from those of the V-phyllosilicates. This suggests that the high-V edge phases are oxides rather than high-V zones in the phyllosilicates. This is supported by Fig. 8, which shows that the spectrum of the edge phase does not show an oxygen K peak as intense as in the roscoelite.

## 4. Discussion

### 4.1. Occurrence of V in phyllosilicates

The scanty literature on V in phyllosilicates generally concludes or assumes that phyllosilicates contain V as crystal lattice substitutions, primarily or entirely as V(iii) in the octahedral layer (Fig. 1) (Foster, 1959; Meunier, 1994; Thorson, 2018; Zheng et al., 2019a, 2022). The data presented here indicate that this is an oversimplification. In fact V exists in phyllosilicates as both distinct V oxide phases and as crystal lattice substitutions. In both cases the V is clearly a mix of V(iii) and V (iv) (Table 6).

The authors are aware of no previous work documenting nanoscale V (-Fe) oxides in phyllosilicates, and thus there is little to compare these results to. However, the results for valence of lattice-substituted V are consistent with the previous analytical data on V in phyllosilicates, though these consist entirely of bulk chemical studies. Foster's (1959) chemical study of mineralized clays from the Colorado Plateau, using acid digestion and titration, found V in eight clay samples as mostly V (iv), with one sample containing a mix of V(iii) and V(iv). This is supported by Wanty and Goldhaber (1985), who developed a colorimetric method to measure V(iii)/V(tot) ratios of two samples from Utah, one of a roscoelite and a second of a V-oxide mineral. Results indicated a V(iii)/V(tot) ratio of 0.85 in the roscoelite and 0.37 for the V oxide. Zanetta et al. (2023) further document a Placerville (CO) roscoelite with a V oxidation state averaging 3.6, from a deposit type and geologic setting similar to those of La Sal. Taken together, these sets of results and our new data strongly suggest that phyllosilicates routinely host a mix of trivalent and tetravalent V.

The location of V in the crystal structure remains unresolved, though Fig. 5 suggests that the tetrahedral as well as the octahedral sites could host significant V as lattice substitutions. This would be consistent with Foster's (1959) observation that both Al and Si contents decrease with increasing V in clays. The remainder of the existing literature is somewhat ambiguous and generally tends to assume substitution on a single site. Meunier (1994) analyzed electron microprobe results showing an inverse Al-V correlation and concluded that V in illites, chlorites, and micas is octahedral; its valence was assumed to be V(iii). Peacor et al. (2000) studied a V-bearing shale from a quarry in Velpen, Indiana with SEM and TEM to characterize V occurrence in the rock. The authors found that V occurred in illite and an illite–smectite solid solution with an overall V content of 1.65 wt% V and a composition of $K_{0.8}(Al_{2.8}Mg_{0.5}Fe_{0.4}V_{0.3})(Si_{7.2}Al_{0.8})O_{20}(OH)_4$. This formula was derived from EDS data and assumed an ideal dioctahedral structure with normalization to 12 tetrahedral plus octahedral cations, with the concomitant assumption that all V existed as octahedral V(iii) (Peacor et al., 2000). This assumption is questionable in view of the points previously discussed. To conclude, the literature clearly indicates that V in phyllosilicates exists between trivalent and tetravalent states and is probably involved in complex multi-site substitions with Si, Al, Mg, and Fe cations.

### 4.2. Correlation of occurrence with leaching behavior

The discovery of a nanoscale high-V oxide edge phase (Fig. 3A-B), with different bonding (Figs. 4 and 5) and metallurgical behavior from the illite, is new information that helps explain why the extraction of V from phyllosilicates is so variable. Tentatively, the results of this study suggest that such nanoscale V-oxide phases provide most of the V recovery from what appear, on a microprobe and larger scale, to be pure V-phyllosilicates. Only grains of the V edge phase that are physically locked in insoluble phyllosilicates, such as the edge phase in Illite Tail 1, do not dissolve. Likewise, the data suggest that V-phyllosilicates with low recoveries are those where these high-V edge phases are scarce to absent and all V is contained in crystallographic sites. The leached residue samples still contain abundant crystallographic V, but lack most or all of the V(-Fe) oxide edge phases in the corresponding unleached heads.

It is not clear from this study's results that either the valence or siting of V substituted on the phyllosilicate lattice has any discernible effect on leaching. EELS results show that V in chlorites is more reduced than V in the illites (Fig. 7, Table 6), which in theory should mean that V in chlorites is slightly more sensitive to oxidation. However, comparisons of STEM-EDS from heads and tails indicate that similarly negligible amounts of crystallographic V were extracted from both illites and

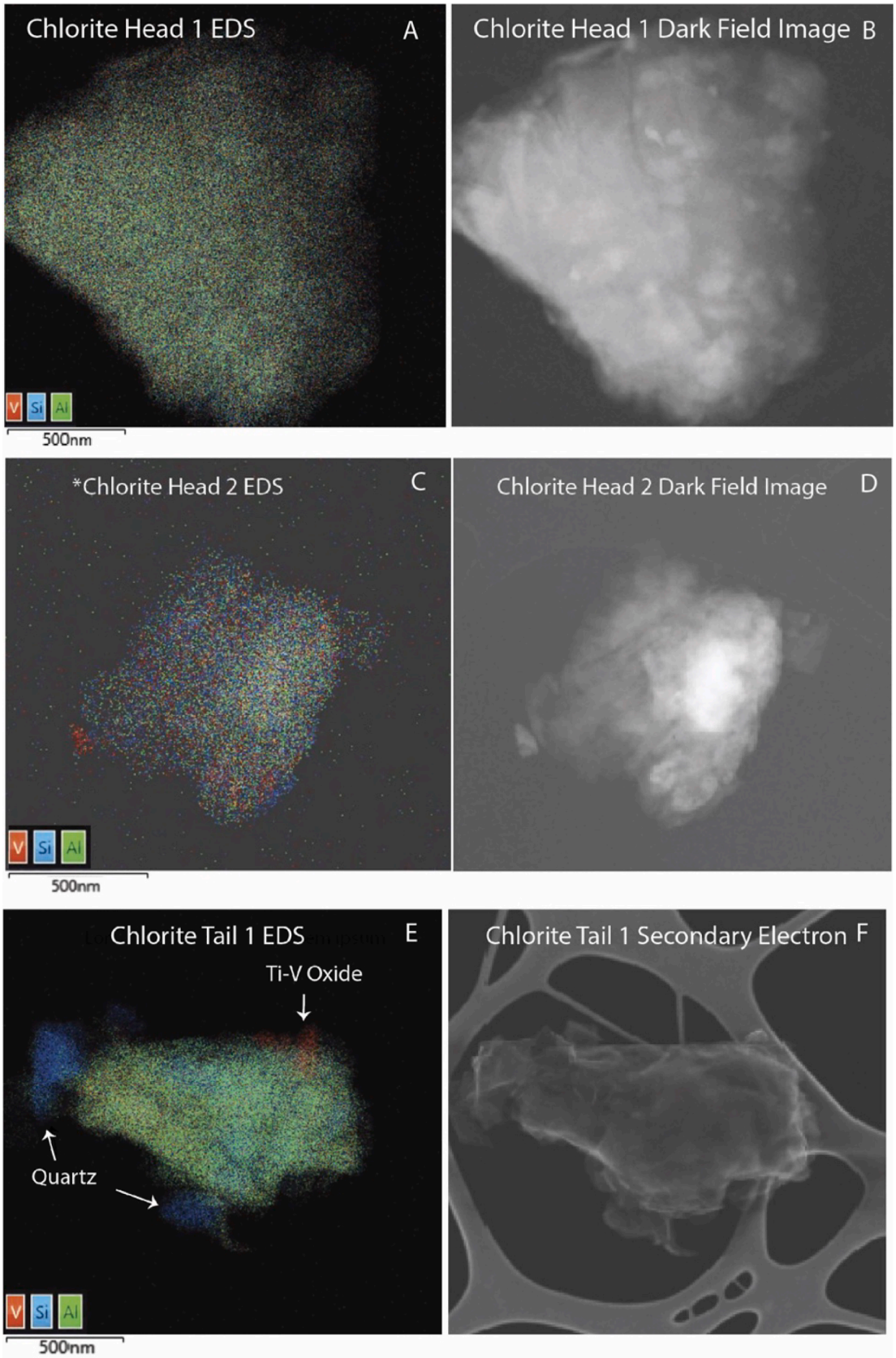


**Fig. 6.** V-Si-Al EDS maps and corresponding electron imaging of V-chlorite (LS04) samples, including heads (A-D) and tails (E-F). * indicates that brightness and contrast have been adjusted for greater legibility in Oxford's AZtec software.

**Table 6**
V oxidation state results determined by EELS.

| Sample | $L_2$ Peak Max Height | $L_2/L_3$ Peak Height | V Oxidation State | $\%V^{3+}$ | $\%V^{4+}$ | $\%V^{5+}$ |
|---|---|---|---|---|---|---|
| $V_2O_3$ standard | 0.9267 | 0.926 | 3.0 | 100.0 | – | – |
| $VO_2$ standard | 0.9876 | 0.987 | 4.0 | – | 100.0 | – |
| $V_2O_5$ standard | 1.0359 | 1.036 | 5.0 | – | – | 100.0 |
| Chlorite Tail Grain 3 (LS04) | 0.9422 | 0.942 | 3.25 | 74.5 | 25.5 | – |
| Chlorite Head 1 (LS04) | 0.9473 | 0.947 | 3.34 | 65.1 | 34.9 | – |
| Chlorite Head 2 (LS04) | 0.9496 | 0.952 | 3.38 | 60.9 | 39.1 | – |
| Roscoelite | 0.9621 | 0.962 | 3.61 | 39.0 | 61.0 | – |
| Illite Tail 1 (LS01) | 0.9663 | 0.966 | 3.69 | 30.3 | 69.7 | – |
| Illite Head 1 (LS01) | 0.9761 | 0.976 | 3.87 | 12.4 | 87.6 | – |
| Illite Tail 2 (LS01) | 0.9792 | 0.979 | 3.92 | 6.7 | 93.3 | – |
| Illite Tail 1V Edge Phase | 0.9794 | 0.979 | 3.93 | 6.3 | 93.7 | – |
| Head V-Oxide (LS04) | 0.9804 | 0.980 | 3.95 | 4.5 | 95.5 | – |

chlorites. Thus there is no clear evidence that V oxidation state or crystal siting affects leaching results.

This contrasts somewhat with the accepted model of silicate dissolution, in which trivalent metals in the octahedral site should leach much faster than lower-coordinated and/or higher-valent metals (Terry, 1983a,b). There is considerable empirical and modeling evidence to support this model at least at the bulk scale (e.g. Brindley and Youell, 1951; Osthaus, 1953; Rozalen et al., 2009), although potential alternative explanations of silicate dissolution exist (reviewed by Crundwell, 2014). The apparent contrast between this conventional model and the results here may be due to several factors. One is the lack of nanoscale characterization accompanying most of the dissolution experiments in the conventional model. Any role played by inclusions of metals or metal oxides in leaching would have gone unnoticed and the metal in solution would have been assumed to come from the phyllosilicate lattice. A second is the strength of the acids used. Chemical dissolution experiments typically use acid concentrations well in excess of the range usual in hydrometallurgy, and favor halide-based over sulfuric acids. The 10 g/L $H_2SO_4$ used to leach the samples examined here was probably far less capable of breaking the stronger chemical bonds in a phyllosilicate (Table 1) than the strong HCl common in dissolution experiments. Thus, while crystal siting of V and other metals likely does affect leaching rates in acids that can break the stronger silicate bonds, it is not clear that this is relevant to the conditions of hydrometallurgical extraction.

One clear conclusion from this study is that a full understanding of process mineralogy and geometallurgy may sometimes require analysis down to the nanoscale. Two ore minerals may look identical at larger scales except for leaching behavior. The case examined here shows that the differences in leachability can relate to differences in mineralogy that are only visible on the nanoscale. Obviously, this complicates recovery predictions. This is particularly the case for complex minerals like phyllosilicates, which can accommodate metal ions in three different ways on the nanoscale, with very different implications for overall recovery.

### 4.3. Implications for the geometallurgy of other V deposits

Phyllosilicates are a significant world V resource, occurring in some sandstone-hosted vanadium (SSV) deposits and in black shale or stone coal deposits (Kelley et al., 2017). These two deposit types between them account for most V resources in the USA and China (Zhang et al., 2011; Kelley et al., 2017). Much to most of the resource is hosted in V-phyllosilicates, though whether as crystallographic V or edge-phase oxides has not been examined.

The extractive metallurgy of the black shale deposits has been a recent focus of investigation (Li et al., 2009; Zhang et al., 2011; Zheng et al., 2019a,b). Studies usually identify the V-bearing silicate as "muscovite," which is the mineral roscoelite or a muscovite with significant V in theory substituting for Al(iii) (Li et al., 2009; Zheng et al., 2019b). Unfortunately, most characterization is not detailed enough to resolve the detailed mineralogy or occurrence of the recovered V (Li et al., 2009; Zheng et al., 2019b). While diagnostic leaching indicates nearly equal components of V(iii), V(iv), and V(v) in some of the black shales, it is unclear how this valence state determination was made or

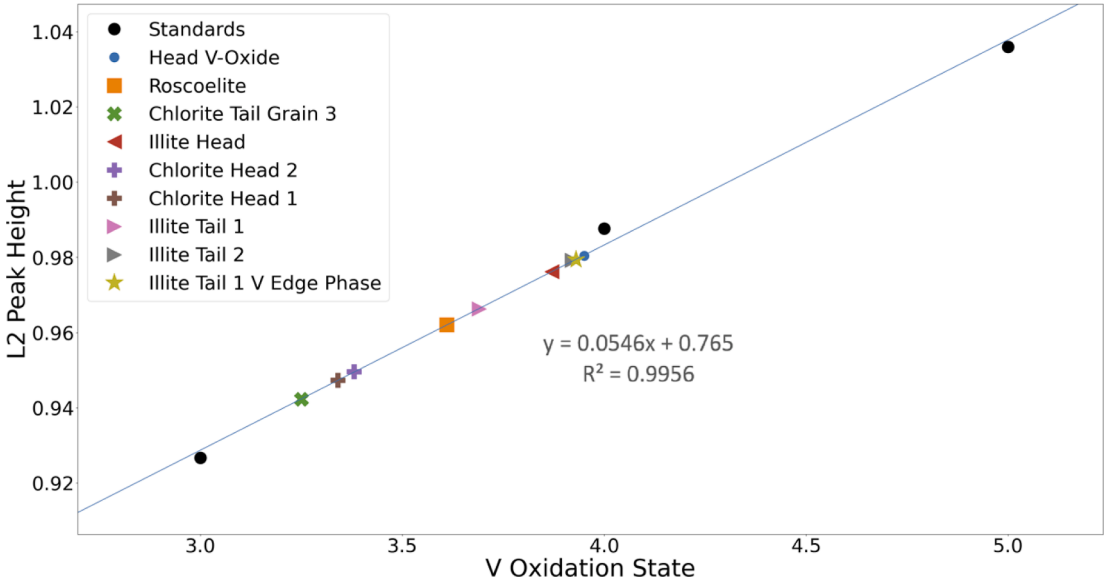


**Fig. 7.** Plot of maximum $L_2$ peak height vs. oxidation state for known V valence $V_2O_3$, $VO_2$, and $V_2O_5$ standards, Placerville roscoelite, and illite and chlorite samples (see section 4.4.3). Illites are from LS01, chlorites from LS04. Trend line is for standards.

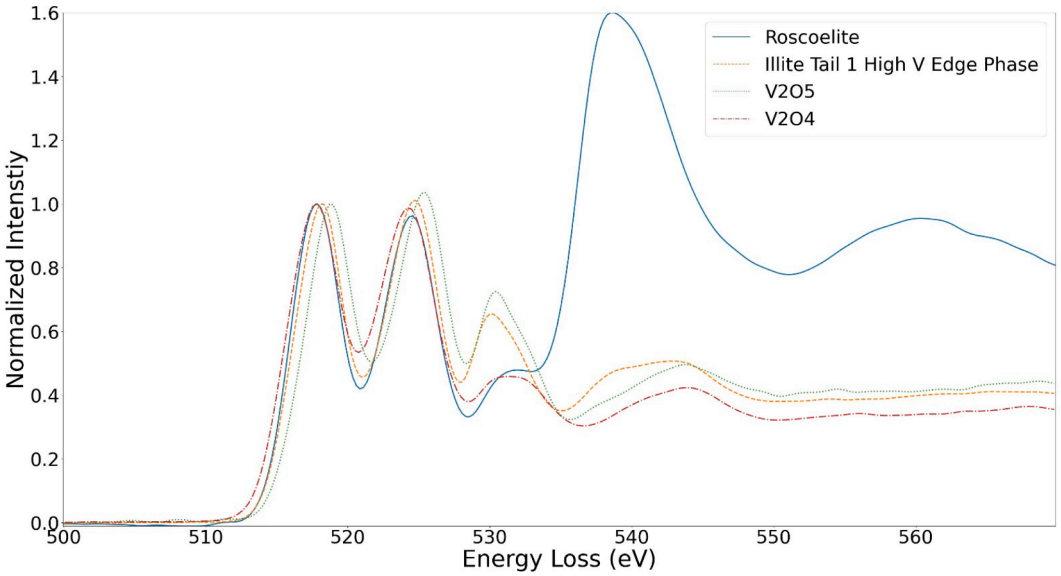


**Fig. 8.** EELS results for the $V_2O_4$ standard, $V_2O_5$ standard, roscoelite, and the high-V edge phase of an illite sample, showing the similarity in O-K edge between the edge phase and the oxides.

what mineral(s) it represents (Li et al., 2009). Detailed modeling and experiments were performed by Zheng et al. (2019a), but though they modeled V crystal chemistry as octahedral V(iii) in a muscovite structure, their leaching experiments indicate that this was not the mineralogy of the sample (SEM-EDS analysis measured almost 18% Mg and < 1% K, more likely a clinochlore than muscovite or roscoelite) (Zheng et al., 2019a,b).

These uncertainties over the mineralogy, V occurrence, and correlation with leachability of V in phyllosilicates in black shale deposits make it difficult to apply our results to them. This study's principal conclusion is that the wide range of reported recoveries and mineral types suggests that those ores, too, could benefit from a closer examination of V occurrence type in the ores.

Whether these results point the way to improved recoveries is uncertain. The unleached V in residues consists of locked V-oxide phases and V bound on the silicate lattice. Practical options for extracting either of these are limited. The ultrafine grinding required to liberate locked V-oxides is prohibitively expensive. Leaching V from the crystal structure would require fluorinated additives that can dissolve the silicate lattice. Although tested in the laboratory (Zheng et al., 2019a), this is unlikely to work in industrial settings. The additives are nonselective and would react with all silicate lattices irrespective of their V content; in sandstone ores, this could include the mainly quartz gangue. The possible creation of hydrofluoric acid from the additives complicates the question further. In some ores it may be possible to increase the temperature or acid concentration during leaching, which might produce incremental improvements.

### 4.4. Implications for other commodities

In addition to hosting major V resources, phyllosilicates are significant in the geometallurgy of other commodities. Phyllosilicate gangue minerals are major long-term reagent consumers in acid leaching of other commodities, like copper (Baum, 1999; Chetty, 2018). Most current practice uses empirical acid consumption testing for predictions, but there are numerous attempts in the literature to develop predictions based on assigning a molar acid consumption value to different mineral types (e.g. Chetty, 2018). As this study shows, this approach, though useful, is an oversimplification. A change in the crystal chemistry can significantly affect metal recovery, it may also apply to metals exchanged for acid in more typical phyllosilicate gangue as well. For instance, the acid consumption of a biotite or chlorite might vary depending on how much of its Fe content is crystallographic and how much consists of nanoscale grains of Fe oxide. The same mineralogical complexities that complicate V recovery are probably just as applicable to the unwanted exchange of metals for leaching reagent in gangue acid consumption.

### 4.5. Conclusion

Metals in phyllosilicates may occur as adsorbed ions, as ions in the crystallographic lattice, or as nanoscopic but discrete grains of metals or metal oxides, and these variations in siting likely affect leaching recoveries. In this case study, the occurrence and valence of V in phyllosilicate ores was examined and correlated with leachability.

The results show that V occurs as (1) crystallographic V(iii) and V(iv) and (2) zones of V oxide or hydroxide on the edges of phyllosilicate grains. These latter are present in some illites but not chlorites, and correlate positively with higher V recovery. They are absent from leached tails, suggesting that the higher V recovery observed in some illite samples is due to the presence of these relatively soluble oxide minerals. In contrast, crystallographic V showed poor extraction in both chlorites and illites without any noticeable effect from either V valence or crystal siting as far as it could be determined. In chlorites V is much more reduced than in V-illites, but this does not correlate with extraction. All V observed in oxides, including the edge phases in phyllosilicates, were relatively oxidized compared to the V hosted in the phyllosilicate lattice proper.

Beyond V extraction, this study indicates that metal leaching from phyllosilicates – whether as targeted ores or in gangue acid consumption – is complex down to a very small scale. Where what appears to be the same mineral phase yields very different metallurgical results, it may be necessary to analyze it on the nanoscale to understand the causes of variability. In addition, this suggests that the common metallurgical practice of assigning a single value to gangue acid consumption based on mineral stoichiometry is overly simplistic and may or may not yield reliable results. The actual metal extracted and acid consumed will vary depending on parameters such as the prevalence of metal and metal oxide phases, their solubility, their location at grain centers or edges, and possibly the coordination and valence state of the crystallographic fraction of the metals. Further work is required to fully understand the prevalence of microscopic metals and metal oxides within phyllosilicate

minerals and the role of metal valence state in determining leachability.

## CRediT authorship contribution statement

**Maxwell Drexler:** Conceptualization, Data curation, Investigation, Formal analysis, Methodology, Writing – original draft, Writing – review & editing, Software, Visualization. **Isabel Barton:** Conceptualization, Data curation, Investigation, Formal analysis, Methodology, Writing – original draft, Writing – review & editing, Funding acquisition, Project administration, Supervision. **Pierre-Marie Zanetta:** Conceptualization, Data curation, Investigation, Formal analysis, Methodology, Writing – original draft, Writing – review & editing, Software, Visualization, Validation.

## Declaration of Competing Interest

The authors declare that they have no known competing financial interests or personal relationships that could have appeared to influence the work reported in this paper.

## Data availability

Data will be made available on request.

## Acknowledgements

We would like to acknowledge Drs. Thomas Zega, Jinhong Zhang, and Brent Hiskey at the University of Arizona for their helpful comments on this work. The Economic Geology and Geometallurgy lab at the UA provided use of the JEOL 6010LA SEM. Drs. Yao-Jen (Jerry) Chang and Zoe Zeszut of the Lunar and Planetary Laboratory provided expert assistance with the Hitachi HF-5000 Transmission Electron Microscope and FEI Helios SEM/FIB, respectively. Energy Fuels Inc., especially Dan Kapostasy, Timo Groves, and Logan Shumway, provided technical assistance as well as access to samples and facilities. We thank the National Science Foundation (NSF) grant #20-54277 for funding this work.

## References

Ahn, J.H., Xu, H., Buseck, P.R., 1997. Transmission electron microscopy of native copper inclusions in illite. Clay Clay Miner. 45, 295–297.

Baker, C.E., Sparling, D.K., 1981. Design and development of the White Mesa uranium mill. Min. Eng. 33, 382–385.

Barton, M.D., Barton, I.F., and Thorson, J.P., 2018a, Paleofluid flow in the Paradox Basin: Introduction. In: Thorson, J.P. (ed.), Paradox Basin fluids and Colorado Plateau copper, uranium and vanadium deposits field trip, Society of Economic Geologists, Guidebook Series, v. 59, p. 1-12.

Barton, I.F., Barton, M.D., Thorson, J.P., 2018b, Characteristics of Cu and U-V deposits in the Paradox Basin (Colorado Plateau) and associated alteration. In: Thorson, J.P. (ed.), Paradox Basin fluids and Colorado Plateau copper, uranium and vanadium deposits field trip, Society of Economic Geologists, Guidebook Series, v. 59, p. 73-102.

Baum, W., 1999. 1999, The use of a mineralogical data base for production forecasting and troubleshooting in copper leach operations: Proceedings of the Copper 99 International Conference. Arizona, Phoenix.

Bleam, W.F., 1993. Atomic theories of phyllosilicates: quantum cheistry, statistical mechanics, electrostatic theory, and crystal chemistry. Reviews of Geophysics 31 (1), 51–73.

Borg, G., Karner, K., Buxton, M., Armstrong, R., Merwe, S.W.v.d., 2003. Geology of the Skorpion supergene zinc deposit, southern Namibia. Econ. Geol. 98 (4), 749–771.

Bos-Orent, E., 2021, Characterization of U(-V) deposits in the La Sal district, UT and CO and their relationship to Paradox Basin fluid flow, Masters Thesis, University of Arizona, Tucson, Arizona, retrieved from repository.arizona.edu.

Brindley, G.W., Youell, R.F., 1951. A chemical determination of 'tetrahedral' and 'octahedral' aluminium ions in a silicate. Acta Crystallogr. 4 (6), 495–496.

Chetty, D., 2018. Acid-gangue interactions in heap leach operations: a review of the role of mineralogy for predicting ore behavior. Minerals v, 8.

Crundwell, F.K., 2014. The mechanism of dissolution of minerals in acidic and alkaline solutions: Part II. Application of a new theory to silicates, aluminosilicates and quartz. Hydrometallurgy 149, 265–275.

Cuney, M., Mercadier, J., Bonnetti, C., 2022. Classification of sandstone-related uranium deposits. J. Earth Sci. 33 (2), 236–256.

Dahlkamp, F.J., 2010. Uranium deposits of the world: USA and Latin America. Springer Reference, Berlin, p. 535.

De La Pena, F., Prestat, E., Fauske, V.T., Burdet, P., Laehnemann, J., Jokubauskas, P., Furnival, T., Nord, M., Ostasevicius, T., MacArthur, K.E., Johnstone, D.N., Sarahan, M., Taillon, J., Aarholt, T., Migunov, V., Eljarrat, A., Caron, J., Francis, C., Nemoto, T., Poon, T., Mazzucco, S., Tappy, N., Cautaerts, N., Somnath, S., Slater, T., Walls, M., Winkler, F., and Anes, H.W., 2021, hyperspy/hyperspy: Release v1.7.2. https://doi.org/10.5281/zenodo.7090040.

Drexler, M.S., 2022, Vanadium in phyllosilicates. Unpublished M.S. thesis, University of Arizona, 58 p.

European Commission, 2020, Critical raw materials resilience: charting a path towards greater security and sustainability. Accessed online 7/18/2022 at https://eur-lex.europa.eu/legal-content/EN/TXT/?uri=CELEX:52020DC0474.

Foster, M.D., 1959. Chemical study of the mineralized clays, in Garrels, R.M. and Larsen, E.S., *Geochemistry and mineralogy of the Colorado Plateau uranium ores*, U.S. Geol. Surv. Prof. Pap. 320, 121–132.

Gao, F., Olayiwola, A.U., Liu, B., Wang, S., Du, H., Li, J., Wang, X., Chen, D., Zhang, Y.i., 2021. Review of vanadium production part I: primary resources. Miner. Process. Extr. Metall. Rev. 43 (4), 466–488.

Gilligan, R., Nikoloski, A.N., 2020. The extraction of vanadium from titanomagnetites and other sources. Miner. Eng. 146, #106106.

Graefe, M., McFarlane, A., Klauber, C., 2017. Clays and the minerals processing value chain (MPVC). In: Gräfe, M., Klauber, C., McFarlane, A.J., Robinson, D.J. (Eds.), Clays in the Minerals Processing Value Chain. Cambridge University Press, pp. 1–80.

Jansen, M., Taylor, A., 2003, Overview of gangue mineralogy issues in oxide copper heap leaching: proceedings of the ALTA Conference, Perth, Australia, 2003, p. 19-24.

Gupta, C.K., 1985. Extractive metallurgy of niobium, tantalum, and vanadium. Int. Met. Rev. 29 (1), 405–444.

Ilton, E.S., Veblen, D.R., 1993. Origin and mode of copper enrichment in biotite from rocks associated with porphyry deposits: a transmission electron microscopy investigation. Econ. Geol. 88, 885–900.

Kear, G., Shah, A.A., Walsh, F.C., 2011, Development of the all-vanadium redox flow battery for energy storage: a review of technological, financial and poly aspects. Int. J. Energy Res., v. 36 pp. 1105-1120.

Kelley, K.D., Scott, C.T., Polyak, D.E., Kimball, B.E., 2017, Vanadium, chap. U *of* Schulz, K.J., DeYoung, J.H., Jr., Seal, R.R., II, and Bradley, D.C., eds., Critical mineral resources of the United States—Economic and environmental geology and prospects for future supply: U.S. Geological Survey Professional Paper 1802, p. U1–U36.

Li, M., Wei, C., Fan, G., Li, C., Deng, Z., Li, X., 2009. Extraction of vanadium from black shale using pressure acid leaching. Hydrometall. 98 (3-4), 308–313.

Meunier, J.D., 1994. The composition and origin of vanadium-rich clay minerals in Colorado-Plateau Jurassic Sandstones. Clay Clay Miner. 42 (4), 391–401.

Moskalyk, R.R., Alfantazi, A.M., 2003. Processing of vanadium: a review. Miner. Eng. 16 (9), 793–805.

Osthaus, B.B., 1953. Chemical determination of tetrahedral ions in nontronite and montmorillonite. Clay Clay Miner. 2 (1), 404–417.

Peacor, D.R., Coveney, R.M., Zhao, G., 2000. Authigenic illite and organic matter: the principal hosts of vanadium in the Mecca Quarry Shale at Velpen, Indiana. Clay Clay Miner. 48, 311–316.

Peters Geosciences, 2014. La Sal District Project NI43-101 Technical Report, 74 p.

Polyak, D., 2018. U.S. Geological Survey Yearbook Vanadium.

Polyak, D., 2021, Vanadium: U.S. Geological Survey, Mineral Commodity Summaries.

Pourbaix, M., 1975. Atlas of electrochemical equilibria in aqueous solutions: Houston. National Association of Corrosion Engineers, p. 643 p..

Radwany, M., 2021. Geometallurgical characterization of sandstone-hosted vanadium ore from the Colorado Plateau. University of Arizona, Tucson, Arizona. Masters Thesis,retrieved from repository.arizona.edu.

Radwany, M.R., Barton, I.F., 2022. The process mineralogy of leaching sandstone-hosted uranium-vanadium ores. Minerals Engineering 187, 107811.

Ross, G.J., 1969. Acid dissolution of chlorites: release of magnesium, iron, and aluminum and mode of acid attack. Clay Clay Miner. 17 (6), 347–354.

Rozalen, M., Huertas, F.J., Brady, P.V., 2009. Experimental study of the effect of pH and temperature on the kinetics of montmorillonite dissolution. Geochim. Cosmochim. Acta 73 (13), 3752–3766.

Terry, B., 1983a. The acid decomposition of silicate minerals part II. hydrometallurgical applications. Hydrometall. 10 (2), 151–171.

Terry, B., 1983b. The acid decomposition of silicate minerals part I. Reactivities and modes of dissolution of silicates. Hydrometallurgy 10 (2), 135–150.

Thorson, 2018, Paradox basin fluids and Colorado Plateau copper, uranium and vanadium deposits: overview. In: Thorson, J.P., Paradox Basin fluids and Colorado Plateau copper, uranium and vanadium deposits field trip, Society of Economic Geologists, Guidebook Series, v. 59, p. 13-46.

Wanty, R., Goldhaber, M., 1985. A method for the determination of vanadium and iron oxidation states in naturally occurring oxides and silicates. Talanta 32 (5), 395–398.

Zanetta, P.-M., Drexler, M.S., Barton, I.F., Zega, T.J., 2023, Vanadium electronic configuration determination from $L_{2,3}$ transition in V-oxide compounds and roscoelite. Am. Mineral. 29(2) 459-469.

Zhang, Y.M., Bao, S.X., Liu, T., Chen, T.J., Huang, J., 2011, The technology of extracting vanadium from stone coal in China: history, current status and future prospects. Hydrometallurgy 109 (2011) 116-124.

Zheng, Q., Zhang, T., Lieu, T., Huang, J., Xue, N., 2019a. Vanadium extraction from black shale: enhanced leaching due to fluoride addition. Hydromatlluergy 187, 141–148.

Zheng, Q., Zhang, Y., Xue, N., Liu, T., Huang, J., 2019b. Vanadium occupation and its leachability differences in trioctahedral and dioctahedral mica. RSC Advances 9 (47), 27615–27624.

## Further reading

Bickmore, B.R., Bosbach, D., Hochella, M.F., Charlet, L., Rufe, E., 2001. In situ atomic force microscopy study of hectorite and nontronite dissolution: Implications for phyllosilicate edge surface structures and dissolution mechanisms. Am. Mineral. 86 (4), 411–423.

Brandt, F., Bosbach, D., Krawczyk-Bärsch, E., Arnold, T., Bernhard, G., 2003. Chlorite dissolution in the acid pH-range: A combined microscopic and macroscopic approach. Geochim. Cosmochim. Acta 67 (8), 1451–1461.

Brigatti, M.F., Caprilli, E., Marchesini, M., Poppi, L., 2003. The crystal structure of roscoelite-1M. Clay Clay Miner. 51, 301–308.

Weeks, A.D., Coleman, R.G., Thompson, M.E., 1959, Part 5. Summary of the ore mineralogy: *in* Garrels, R.M., and Larsen, E.S. (eds.), Geochemistry and mineralogy of the Colorado Plateau Uranium Ores, US Geological Survey Professional Paper 320, p. 65-80.

Kalinowski, B.E., Schweda, P., 1996. Kinetics of muscovite, phlogopite, and biotite dissolution and alteration at pH 1–4, room temperature. Geochim. Cosmochim. Acta 60 (3), 367–385.

Kociak, M., Stéphan, O., Walls, M.G, Tencé, M., Colliex, C., 2011. Spatially resolved EELS: The spectrum-imaging technique and its applications, in Pennycook, S.J., and Nellist, D.P., eds., Scanning Transmission Electron Microscopy, 1st ed.: New York, Springer New York, p. 163-205.

Slick, L.R., Chang, Y.-J., Zega, T., 2019. Calculation of chemical shift for Ti via EELS white-line-ratio method. Microscopy Microanal. 25 (S2), 662–663.

Snäll, S., Liljefors, T., 2000. Leachability of major elements from minerals in strong acids. J. Geochem. Explor. 71 (1), 1–12.

Tan, H., Verbeeck, J.o., Abakumov, A., Tendeloo, V.G., 2012. Oxidation state and chemical shift investigation in transition metal oxides by EELS. Ultramicroscopy 116, 24–33.

Tavakoli, M.R., Dornian, S., Dreisinger, D.B., 2014. The leaching of vanadium pentoxide using sulfuric acid and sulfite as a reducing agent. Hydrometall. 141, 59–66.